

MAJOR PAPER

Demonstration of Human Fetal Bone Morphology with MR Imaging: A Preliminary Study

Yoshiko Matsubara^{1*}, Toru Higaki¹, Chihiro Tani², Shogo Kamioka³,
Kuniaki Harada⁴, Hirohiko Aoyama⁵, Yuko Nakamura¹, Tomoyuki Akita⁶,
and Kazuo Awai¹

Purpose: CT is a useful modality for the evaluation of fetal skeletal dysplasia but radiation exposure is unavoidable. The purpose of this study is to compare the usefulness of MRI and CT for evaluating the fetal skeletal shape.

Methods: This study was approved by our Institutional Review Board. Fetal specimens ($n = 14$) were scanned on a 3T MRI scanner using our newly-developed sequence. It is based on T_2^* -weighted imaging (TR, 12 ms; TE for opposed-phase imaging, 6.1 ms, for in-phase imaging, 7.3 ms; flip angle, 40°). The specimens were also scanned on a 320 detector-row CT scanner. Four radiologists visually graded and compared the visibility of the bone shape of eight regions on MRI- and CT-scans using a 5-point grading system.

Results: The diagnostic ability of MRI with respect to the 5th metacarpals, femur, fibula, and pelvis was superior to CT (all, $P < 0.050$); there was no significant difference in the evaluation results of observers with respect to the cervical and lumbar spine, and the 5th metatarsal ($0.058 \leq P \leq 1.000$). However, the diagnostic ability of MRI was significantly inferior to CT for the assessment of the bone shape of the thoracic spine (observers A and C: $P = 0.002$, observers B and D: $P = 0.001$).

Conclusion: The MRI method we developed represents a potential alternative to CT imaging for the evaluation of the fetal bone structure.

Keywords: bone diseases, fetal specimen, magnetic resonance imaging, prenatal diagnosis, radiation exposure

Introduction

Fetal skeletal dysplasia is a heterogeneous anomaly comprised of more than 400 disorders associated with bone and cartilage disorders. It affects fetal skeletal formation and results in an anomalous shape and size and compromised

skeletal integrity. Although the incidence of each disorder is low, the rate of skeletal dysplasia is close to one in 5000 births.¹ A prenatal diagnosis is important for selecting the delivery method and for early intervention.²

Ultrasonography (US) is the first-line imaging modality to screen fetuses. While the diagnostic accuracy of 2D US for fetal skeletal dysplasia ranges from only 40–60%,^{3,4} on CT scans, the whole fetal skeleton is visualized.^{4–9} Therefore, CT is considered to be valuable for the prenatal diagnosis of skeletal dysplasia.^{6,8–10} However, radiation exposure at CT is a critical issue as fetuses are more radiation-sensitive than adults^{11,12} and low radiation doses may result in DNA double-strand breaks.¹³ Although some low-dose CT scanning techniques have been developed,^{6,8–10} radiation exposure is unavoidable.

MRI is a possible alternative for the examination of the fetal skeletal system.^{14,15} It demonstrates the bone cortex as a low-intensity area due to the absence of hydrogen protons; as T_2 or T_2^* relaxation time is very short it can be difficult to differentiate surrounding tissues from the bone cortex. We devised a MR sequence based on a T_2^* -weighted scan sequence that can identify the bone structure and differentiate

¹Department of Diagnostic Radiology, Graduate School of Biomedical and Health Sciences, Hiroshima University, 1-2-3 Kasumi, Minami-ku, Hiroshima, Hiroshima 734-8553, Japan

²Department of Diagnostic Radiology, Hiroshima City Hospital, Hiroshima, Japan
³Department of Diagnostic Radiology, Hiroshima University Hospital, Hiroshima, Japan

⁴Healthcare Business Unit, Hitachi, Ltd., Tokyo, Japan

⁵Department of Medical Science and Technology, Faculty of Health Sciences, Hiroshima International University, Hiroshima, Japan

⁶Department of Epidemiology, Infectious Disease Control and Prevention, Graduate School of Biomedical and Health Sciences, Hiroshima University, Hiroshima, Japan

*Corresponding author, Phone: +81-82-257-5257, Fax: +81-82-257-5259, E-mail: matsuy@hiroshima-u.ac.jp

©2019 Japanese Society for Magnetic Resonance in Medicine
This work is licensed under a Creative Commons Attribution-NonCommercial-NoDerivatives International License.

Received: April 25, 2019 | Accepted: September 7, 2019

it from surrounding tissue. In this preclinical study we used human fetal specimens to investigate whether MRI is an alternative to CT for the evaluation of the fetal bone shape.

Materials and Methods

This cross-sectional study was approved by our Institutional Review Board. Written informed consent was waived because the human fetal specimens had been stored in formalin for 50–60 years; consequently it was impossible to identify relatives.

Specimens

We acquired 14 fetal specimens from our Department of Anatomy; they had been stored for educational and research purposes. We selected specimens with a gestational age of 28–32 weeks because they were well preserved and because fetal CT is generally performed in the 2nd or 3rd trimester to minimize adverse irradiation-related sequelae.⁵ Our determination of the fetal age was based on the crown-rump length.¹⁶ The 14 specimens were five males and nine females; four were at 28- and the other 10 at 32-week gestation. Their median weight was 1152 g (range, 601–1576 g).

We placed each fetus in a cylindrical plastic container (length, 27 cm; diameter, 23 cm) filled with water. To secure each specimen in the container, we placed it on a plastic base and surrounded it with a plastic net. We also inserted a plastic tube and bottles containing oil in the container (Fig. 1).

Before MRI we confirmed the absence of bone demineralization and skeletal dysplasia on prior CT scans.

MRI

We used a 3T MRI scanner (TRILLIUM OVAL, Hitachi, Tokyo, Japan). Because 3D image processing was of importance, to demonstrate the bone shape accurately, we optimized the T_2^* -weighted multiple gradient-echo sequence by selecting TE and flip angle that yielded high contrast between bones and surrounding tissues. We also removed the black band arising from chemical shift artifacts to avoid bone shape overestimation. For details see Supplementary Material. The parameters for our MRI studies were TR, 12 ms; TE for opposed-phase imaging, 6.1 ms; in-phase imaging, 7.3 ms; flip angle, 40°; band width, 182 kHz; scan FOV, 300 mm; frequency matrix, 428; slice thickness, 1.2 mm (axial plane); slice spacing, 0.6 mm; number of excitations (NEX), 1. The scan time was 10 min and 58 s.

CT

We acquired helical scans on a 320-detector row CT scanner (Aquilion One Genesis version, Canon Medical Systems, Tochigi, Japan). The scan parameters were tube voltage, 80 kV; tube current, 800 mA; rotation time, 0.35 s; pitch factor, 1.388; scan FOV, 32 cm; display FOV, 26 cm; detector configuration, 80 × 0.5 mm; reconstruction slice thickness and interval, 0.5 mm. We adopted a fixed tube current and did not

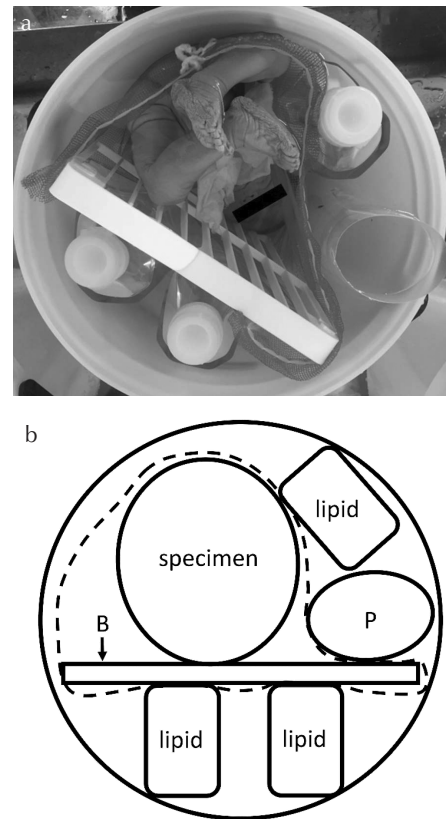


Fig. 1 Experimental set-up. (a) The fetal specimens were placed in a 23-cm diameter plastic container. (b) Schematic drawing. The dashed line indicates the plastic net around the specimen. The arrow points to the plastic base. B: plastic base, lipid: plastic bottles containing oil, p: plastic tube.

use automatic exposure control. Image reconstruction was with a hybrid-type iterative reconstruction algorithm (Adaptive iterative dose reduction, 3D, Canon Medical Systems); the reconstruction kernel was filter convolution (FC) 13 (standard body kernel).

Image analysis

We examined 14 fetal specimens and selected eight regions (cervical spine, thoracic spine, lumbar spine, 5th metacarpals, 5th metatarsals, femurs, fibulas, pelvis) for evaluation on MRI scans. We included the spine because its evaluation by US is difficult although inspection of the spine is indispensable for the diagnosis of skeletal dysplasia. The 5th metacarpals and metatarsals represent the small-, and the fibulas and femurs the long bones.

To evaluate the MRI scans, we generated curved planar reconstruction (CPR) images along the long axis of the bones. Our standard images were maximum intensity projection (MIP) images obtained by CT. The display window and level of the CT images was as in “bone window”. The window level was 400, the width was 840–1200. To evaluate the pelvis we used volume-rendering (VR) images. CPR, MIP, and VR images were generated on a workstation

(Virtual Place Fujin 370, version 3.7011, AZE, Tokyo, Japan). Four board-certified radiologists with 17, 33, 10, and 10 years of experience in radiology assessed demonstration of the fetal bones on MRI scans. Visualization of the bones on MRI scans was scored using CT images as the reference standard. The 5-point scoring system was based on the Likert scale.^{17,18}

The diagnostic performance of MR and CT images with respect to bone sharpness and morphology was compared and graded as 5 = MRI definitely superior, 4 = MRI slightly superior, 3 = MRI and CT almost the same, 2 = MRI slightly inferior to CT but diagnosis possible, 1 = MRI definitely inferior (Figs. 2 and 3).

Statistical analysis

The quality of the MRI scans was visually evaluated by applying the McNemar test to the eight examined regions. When the *P*-value was <0.05 and the number of specimens with a score of 4 or 5 exceeded that of specimens with a score of 1 or 2, we considered the diagnostic ability of MRI superior to CT. On the other hand, when the *P*-value was <0.05 and the number of specimens with a score of 1 or 2 exceeded that of specimens with a score of 4 or 5, we recorded the diagnostic ability of CT superior to MRI.

Interobserver agreement was analyzed using weighted kappa statistics, where κ -coefficient < 0.10 = poor, 0.21–0.40 = fair, 0.41–0.60 = moderate, 0.61–0.80 = substantial, 0.81–1.00 = almost perfect agreement.¹⁹ Statistical analysis was performed with statistical software (R package version 3.4.1, JMP Pro, version 13.0.0, SAS Institute Inc., Cary, NC, USA).

Results

Table 1 show the visualization scores assigned to the MRI scans by the four readers to eight areas in 14 fetal specimens. By all readers, only visualization of the thoracic spine was recorded as inferior on MRI than CT scans (score 1 or 2). These results indicate that only with respect to the bone shape of the thoracic spine, the diagnostic ability of MRI was inferior to CT. The readers reported that on MRI scans of the thoracic spine assigned a score of 2, the signal intensity of the intervertebral disks was as low as that of the vertebral bodies, rendering their differentiation difficult (Fig. 3b). On the other hand, with respect to visualization of the 5th metacarpal, femur, fibula, and pelvis, their visualization was reported as significantly better on MRI than CT scans (Fig. 3c–3f).

The κ -coefficient for interobserver agreement for the cervical spine, lumbar spine and fibula was moderate (0.59, 0.55, and 0.55, respectively). It was substantial for the other five areas (range, 0.68–0.76) (Table 2).

Discussion

Our study demonstrates that our newly-developed MRI sequence yielded visualization of fetal skeletal formation. Small bones, i.e. the 5th metacarpal and the 5th metatarsal

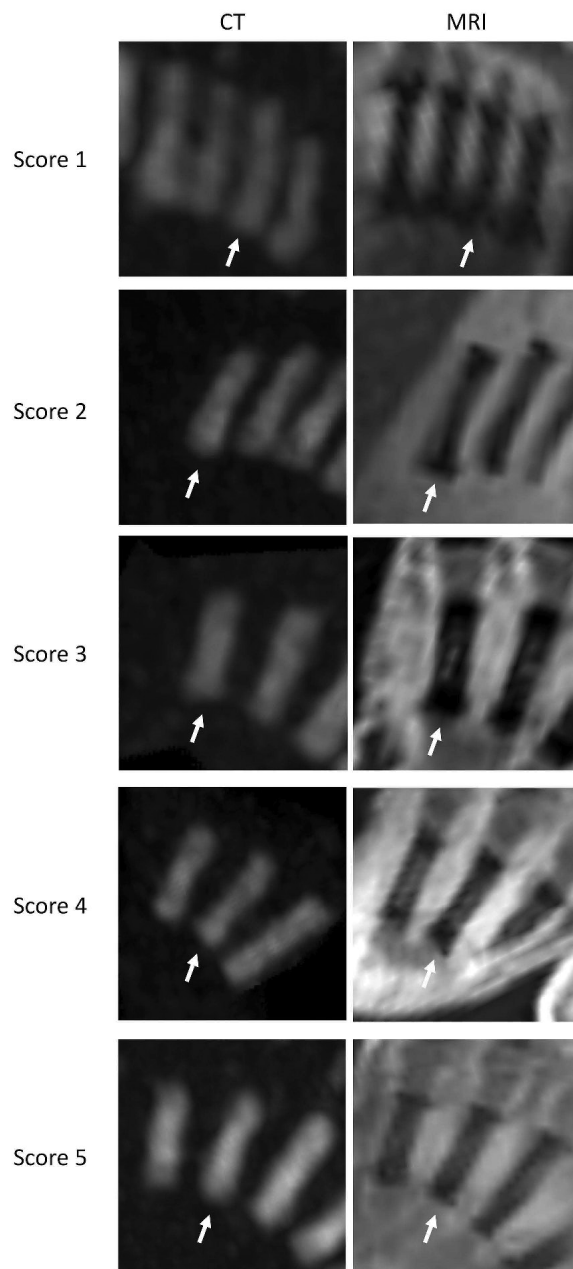


Fig. 2 Examples of the visualization scores. Score 1: The metatarsal bone (arrows) is blurred but confirmed. The bone contour is uncertain on the MRI scan. MRI is definitely inferior to CT. Score 2: The metatarsal bone (arrows) is blurred on the MRI scan but its contour can be identified. Score 3: The shape and edge of the metacarpal bone (arrows) are the same on CT- and MRI-scans. Score 4: The shape and edge of the metacarpal bone (arrows) are clearer on the MRI- than the CT-scan. Score 5: The edge of the metacarpal bone (arrows) is blurred on the CT image but is clearly visualized on the MRI scan.

and thin bones, e.g. the fibula were clearer on MRI than CT scans. Although the image quality of MRI was inferior to CT for visualization of the thoracic spine, no observer recorded MRI as definitely inferior to CT (score 1), indicating that the diagnostic ability of MRI and CT scans was comparable.

Table 1 Visualization scores recorded by the four observers for the eight regions

	Score (%)					P-value
	1	2	3	4	5	
(a) Observer A						
Cervical spine	0 (0)	1 (7)	6 (43)	6 (43)	1 (7)	0.034
Thoracic spine	0 (0)	10 (71)	4 (29)	0 (0)	0 (0)	0.002
Lumbar spine	0 (0)	1 (7)	10 (71)	2 (14)	1 (7)	0.317
5th metacarpal	0 (0)	0 (0)	6 (43)	6 (43)	2 (14)	0.005
5th metatarsal	0 (0)	1 (7)	7 (50)	6 (43)	0 (0)	0.059
Femur	0 (0)	0 (0)	3 (21)	9 (64)	2 (14)	0.001
Fibula	0 (0)	0 (0)	7 (50)	6 (43)	1 (7)	0.008
Pelvis	0 (0)	1 (7)	2 (14)	4 (29)	7 (50)	0.004
(b) Observer B						
Cervical spine	0 (0)	2 (14)	4 (29)	7 (50)	1 (7)	0.058
Thoracic spine	0 (0)	11 (79)	3 (21)	0 (0)	0 (0)	0.001
Lumbar spine	0 (0)	2 (14)	9 (64)	2 (14)	1 (7)	0.655
5th metacarpal	0 (0)	1 (7)	4 (29)	8 (57)	1 (7)	0.011
5th metatarsal	0 (0)	0 (0)	6 (43)	8 (57)	0 (0)	0.005
Femur	0 (0)	0 (0)	3 (21)	9 (64)	2 (14)	0.001
Fibula	0 (0)	0 (0)	6 (43)	7 (50)	1 (7)	0.005
Pelvis	0 (0)	1 (7)	3 (21)	5 (36)	5 (36)	0.007
(c) Observer C						
Cervical spine	0 (0)	1 (7)	4 (29)	8 (57)	1 (7)	0.011
Thoracic spine	0 (0)	10 (71)	4 (29)	0 (0)	0 (0)	0.002
Lumbar spine	0 (0)	0 (0)	8 (57)	5 (36)	1 (7)	0.014
5th metacarpal	0 (0)	0 (0)	4 (29)	8 (57)	2 (14)	0.002
5th metatarsal	0 (0)	0 (0)	6 (43)	8 (57)	0 (0)	0.005
Femur	0 (0)	0 (0)	2 (14)	9 (64)	3 (21)	0.001
Fibula	0 (0)	0 (0)	4 (29)	9 (64)	1 (7)	0.002
Pelvis	0 (0)	0 (0)	3 (21)	3 (21)	8 (57)	0.001
(d) Observer D						
Cervical spine	0 (0)	2 (14)	7 (50)	4 (29)	1 (7)	0.10
Thoracic spine	0 (0)	12 (86)	2 (14)	0 (0)	0 (0)	0.001
Lumbar spine	0 (0)	2 (14)	10 (71)	1 (7)	1 (7)	1.000
5th metacarpal	0 (0)	1 (7)	3 (21)	9 (64)	1 (7)	0.007
5th metatarsal	0 (0)	0 (0)	8 (57)	6 (43)	0 (0)	0.014
Femur	0 (0)	0 (0)	4 (29)	7 (50)	3 (21)	0.002
Fibula	0 (0)	0 (0)	5 (36)	8 (57)	1 (7)	0.003
Pelvis	0 (0)	0 (0)	3 (21)	6 (43)	5 (36)	0.001

Based on these results we suggest that MRI is a potential alternative to CT for the evaluation of fetal bones.

MR sequences that demonstrate the bone shape as a “black bone” in fetuses and children have been reported. Eley et al.²⁰ compared “black bone” visualization of the pediatric cranial bone on MRI and CT scans. Robinson et al.²¹ reported that the fetal spine was observable on

susceptibility-weighted images. However, demonstration of the bone structure of in situ fetuses on MRI and CT scans has not been compared due to ethical issues related to radiation exposure.

Our MRI sequence facilitates the acquisition of high spatial-resolution 3D images of the fine structure of bones. The contrast between bone and the surrounding tissue is higher than

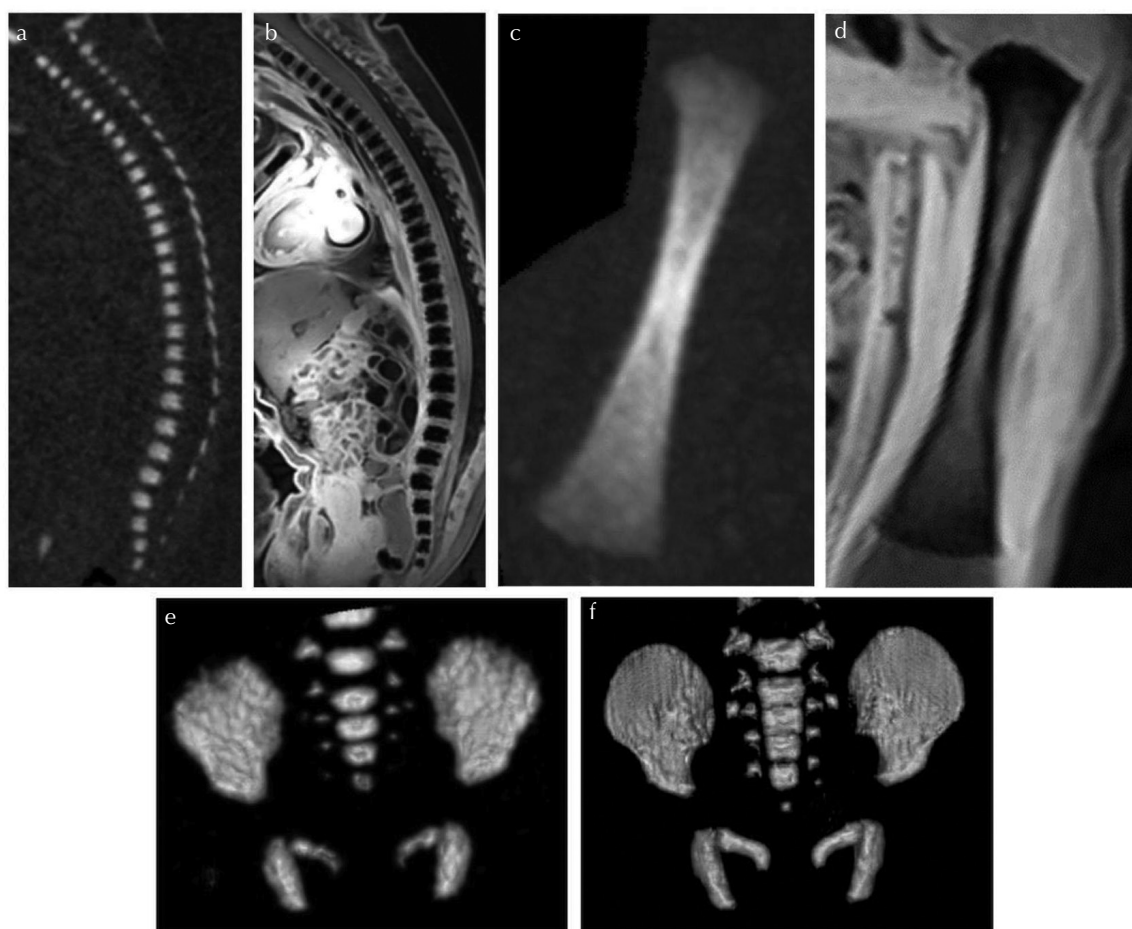


Fig. 3 Examples of fetal images (gestational age 32 weeks). (a) CT, (b) MRI, (c) CT, (d) MRI, (e) CT, (f) MRI. (a and b) Sagittal images of a fetal spine. All observers assigned a visual score of 5 to the cervical spine, of 3 to the thoracic spine, and of 5 to the lumbar spine. On the MRI scan (b) the edge and shape of the cervical and lumbar spine are more clear than on the CT image. (c and d) Coronal images of a fetal femur. All observers assigned a visualization score of 4. On both images the bone edge and morphology are visualized. The structure of the metaphysis is clear on the MRI scan (d). (e and f) Volume-rendered image of a fetal pelvis. All observers assigned a visualization score of 5. The edge of the iliac crest and pubic bone is clearer on the MRI- (f) than the CT-image (e).

Table 2 Interobserver agreement

Bones	κ -Coefficient
Cervical spine	0.59
Thoracic spine	0.76
Lumbar spine	0.55
5th metacarpals	0.72
5th metatarsals	0.68
Femur	0.75
Fibula	0.55
Pelvis	0.69

on scans obtained with ultrashort TE and zero TE (ZTE) sequences. Both involve chemical shift of lipid and inhomogeneity of the static magnetic field resulting in concentric blurring on images due to radial sampling, gridding errors in radial sampling that lead to image deterioration, and the need for

more excitations when radial rather than Cartesian sampling is applied to obtain the same spatial resolution. Also, as the ZTE sequence requires dedicated hardware, its wide-spread application may be limited.²² Therefore, we think that our method makes the best use of the advantages of the Cartesian sampling by adding a correction for the chemical shift of lipid.

Overall, interobserver agreement was acceptable. For the cervical spine, lumbar spine, and fibula it was moderate, for the other five regions it was substantial. Therefore we concluded that the quality of our fetal MRI scans was stable and of potential clinical applicability.

With our MRI sequence, it was difficult to separate the thoracic spine from connected intervertebral disks because some intervertebral disks were of the same intensity as the bone cortex and water; this made it difficult to differentiate between the vertebral body and vertebral disks. The center of the intervertebral disk, the nucleus pulposus, is highly cellular and contains proteoglycan. As the fetal nucleus pulposus is hydrated and contains a large amount of proteoglycans, the

vertebral disk shows the same intensity as does water.^{23,24} This may explain why our observers were unable to differentiate between the vertebral body and vertebral disks.

As we aimed at obtaining high contrast and high spatial-resolution images, approximately 11 min were required to scan the whole fetus. We think that the scan time can be reduced by fast-imaging techniques. We estimate that the fetal scan time can be shortened by 60% to about 3 min by applying $k_y - k_z$ circular sampling and compressed sensing.^{25–27} Moreover, our image reconstruction method that applies deep learning shortens the time required for image reconstruction time.²⁸ Investigations are underway to determine whether the combination of $k_y - k_z$ circular sampling, compressed sensing, and our image reconstruction method can shorten the image acquisition time to below 3 min.

Although we were able to obtain partial 3D VR images of the pelvis, we could not acquire whole-body 3D VR images because the difference in the signal intensity of the skeletal system and surrounding tissue was insufficient for the generation of such images. While the whole fetal skeletal structure can be observed on 3D VR images,¹⁰ the diagnosis of skeletal dysplasia requires the separate assessment of individual portions. As our scan sequence facilitated the acquisition of fetal volume data, it made possible the evaluation of individual parts and of the whole fetal skeletal structure.

Our study has a limitation. Our findings cannot be extrapolated to *in situ* fetuses because our specimens had been formalin-fixed for more than 50 years. Although CT studies confirmed that their bones were not decalcified, formalin fixes proteins by binding- and cross-linking steps; consequently, most of the organs are degenerated.²⁹ As it is especially difficult to fix fat tissue, it appeared to be less than in *in situ* fetuses.³⁰ According to Haga et al.,³¹ T_2 and T_2^* values of the brain *in vivo* were not significantly different from that with formalin fixation. On the other hand, Birkel et al. showed that formalin fixation reduces the relaxation time of T_1 , T_2 , and T_2^* in the brain. If this applies to other organs, there may be difference in the signal intensity of bone and other organs.²⁹ However, we think that the signal intensity difference between skeletal systems and surrounding tissue can be recognized because in our chicken phantom study we observed a marked difference between bones and peripheral organs (see Supplementary Material).

Conclusion

In conclusion, for the evaluation of the fetal bone shape, the MRI sequence we developed may represent an alternative to CT imaging and may help to diagnose fetal skeletal dysplasia without the risk inherent in radiation exposure.

Funding

This study has received funding by JSPS KAKENHI grant no. 18K15591.

Conflicts of Interest

Kazuo Awai obtained a research grant from Hitachi Co. Ltd. paid to our institution. Kuniaki Harada, an employee of Hitachi Ltd., neither analyzed nor controlled the data used in this study. He contributed to our study by developing the MR scan sequences. The other authors declared no competing interests.

Supplementary Material

Supplementary Figs. 1–3 and Table 1 are available online.

On T_2^* -weighted images, tissues with short T_2 and T_2^* , i.e. bones and tendons, are observed as low-intensity areas. Therefore we optimized our sequence for T_2^* -weighted imaging to demonstrate bone accurately.

Supplementary Fig. 1

Schematic drawing of our method to cancel out the effect of fat tissue. On conventional images there are chemical shift artifacts around the bone cortex that may result in overestimation of the bone cortex. We used the Dixon method to acquire dual-echo acquisition-time images. From in- and out-of-phase images, we acquired water and fat images and translated the fat images in one pixel into the frequency-encoded direction to synthesize fat and water images. TE: echo time.

Supplementary Fig. 2

Images of the chicken phantom acquired with our method for cancelling the effect of fat tissue. Note the black band from the chemical shift artifact at the edge of the bone cortex (solid arrow, top row). Application of our method cancelled the effect of the chemical shift artifact [open arrow (bottom row, right)]. TE: echo time.

Supplementary Fig. 3

Matrix views of images obtained with various TE and FA combinations. TE was the intermediate value of TE on in- and out-of-phase images. Increasing TE increased the contrast between the bone cortex and surrounding tissue. Bottom row: TE for opposed-phase imaging, 6.1 ms; in-phase imaging, 7.3 ms, FA 40° (red frame). TE: echo time, FA: flip angle.

Supplementary Table 1

Contrast-to-noise ratio between the bone cortex and gluteus muscle

Subjects

We used an edible whole chicken as a phantom to optimize the MR sequence. The weight of the chicken was 906 g, almost the same as of a fetus with a gestational age of 24–27 weeks. We placed the chicken phantom in an ellipsoidal plastic box and fixed it with agar.

MRI

We used the same 3T MRI scanner (TRILLIUM OVAL) as in the study of human fetal specimens.

First, to obtain clear bone-cortex images exhibiting high contrast with surrounding tissues, we optimized the T_2^* -weighted multiple gradient-echo sequence. We changed the TE and flip angle (FA).

Cycle 1: TE for opposed-phase imaging, 1.2 ms; in-phase imaging, 2.4 ms.

Cycle 2: TE for opposed-phase imaging, 3.7 ms; in-phase imaging, 4.9 ms.

Cycle 3: TE for opposed-phase imaging, 6.1 ms; in-phase imaging, 7.3 ms.

Cycle 4: TE for opposed-phase imaging, 8.6 ms; in-phase imaging, 9.8 ms.

We also changed the FA to 10-, 20-, 30-, and 40°. The other scan parameters were: TR, 12 ms; band width, 220.0 kHz; scan FOV, 250 mm; frequency matrix, 280; slice thickness, 1.0 mm (coronal plane), NEX 1.

Then we produced synthesized T_2^* images to remove chemical shift artifacts. We used water and fat images because on T_2^* -weighted images, the bone cortex may be over-estimated due to chemical shift artifacts resulting from fat tissue around the bone (Figs. S1 and S2). For TE and FA optimization we used the 2-point Dixon method whose application yielded water- and fat images. We adjusted the MR scan parameters to render the width of chemical shift artifacts to be one pixel (bandwidth 182 kHz, FOV 300 mm, frequency matrix, 428). Then we parallel-translated the fat-phase images in one pixel into the frequency-encoded direction and synthesized fat and water images. Figure S1 is a schematic drawing of our method and Fig. S2 shows actual MR images for each process.

Analysis

We measured the contrast-to-noise ratio (CNR) on each scan. CNR was defined as:

$$\text{CNR} = \text{Intensity (bone)} - \frac{\text{Intensity (muscle)}}{\text{Noise (muscle)}}$$

We measured the signal intensity of bone and of the gluteal muscle at the left proximal diaphysis of the tibia and at the muscle, respectively. As most bones are surrounded by muscle, we defined noise as the standard deviation of the gluteal muscle.

Optimization results

We were unable to obtain a 4th-cycle image due to the limited conditional tolerance of our MRI scanner. Table S1 shows our CNR measurements. The highest CNR (6.88) was obtained at TE 6.7 ms and FA 40°. Figure S3 presents matrix views of images obtained with various combinations of TE and FA.

References

1. Krakow D, Rimoin DL. The skeletal dysplasias. *Genet Med* 2010; 12:327–341.
2. Krakow D, Lachman RS, Rimoin DL. Guidelines for the prenatal diagnosis of fetal skeletal dysplasias. *Genet Med* 2009; 11:127–133.
3. Parilla BV, Leeth EA, Kambich MP, Chilis P, MacGregor SN. Antenatal detection of skeletal dysplasias. *J Ultrasound Med* 2003; 22:255–258; quiz 259–261.
4. Doray B, Favre R, Viville B, Langer B, Dreyfus M, Stoll C. Prenatal sonographic diagnosis of skeletal dysplasias. A report of 47 cases. *Ann Genet* 2000; 43:163–169.
5. Victoria T, Epelman M, Coleman BG, et al. Low-dose fetal CT in the prenatal evaluation of skeletal dysplasias and other severe skeletal abnormalities. *AJR Am J Roentgenol* 2013; 200:989–1000.
6. Miyazaki O, Nishimura G, Sago H, Horiuchi T, Hayashi S, Kosaki R. Prenatal diagnosis of fetal skeletal dysplasia with 3D CT. *Pediatr Radiol* 2012; 42:842–852.
7. Ruano R, Molho M, Roume J, Ville Y. Prenatal diagnosis of fetal skeletal dysplasias by combining two-dimensional and three-dimensional ultrasound and intrauterine three-dimensional helical computer tomography. *Ultrasound Obstet Gynecol* 2004; 24:134–140.
8. Tani C, Funama Y, Fujioka C, et al. Radiation dose reduction at MDCT with iterative reconstruction for prenatal diagnosis of skeletal dysplasia: preliminary study using normal fetal specimens. *AJR Am J Roentgenol* 2014; 203:1249–1256.
9. Imai R, Miyazaki O, Horiuchi T, et al. Ultra-low-dose fetal CT with model-based iterative reconstruction: a prospective pilot study. *AJR Am J Roentgenol* 2017; 208:1365–1372.
10. Adler-Levy Y, Yagel S, Nadjari M, Bar-ziv Y, Simanovsky N, Hiller N. Use of low dose computed tomography with 3D reconstructions for the prenatal evaluation of suspected skeletal dysplasia. *Isr Med Assoc J* 2015; 17:42–46.
11. Willis CE, Slovis TL. The ALARA concept in pediatric CR and DR: dose reduction in pediatric radiographic exams—a white paper conference executive summary. *Pediatr Radiol* 2004; 34:S162–S164.
12. Streffer C, Shore R, Konermann G, et al. Biological effects after prenatal irradiation (embryo and fetus). A report of the International Commission on Radiological Protection. *Ann ICRP* 2003; 33:5–206.
13. Halm BM, Franke AA, Lai JF, et al. γ -H2AX foci are increased in lymphocytes in vivo in young children 1 h after very low-dose X-irradiation: a pilot study. *Pediatr Radiol* 2014; 44:1310–1317.
14. Suzumura H, Kohno T, Nishimura G, Watanabe H, Arisaka O. Prenatal diagnosis of hypochondrogenesis using fetal MRI: a case report. *Pediatr Radiol* 2002; 32:373–375.
15. Nemeč SF, Nemeč U, Brugger PC, et al. MR imaging of the fetal musculoskeletal system. *Prenat Diagn* 2012; 32: 205–213.
16. Shimamura A. [Measurements of physical size and estimation of embryonic age in the Japanese fetuses.] *Leg Med* 1957; 11:795–811 (in Japanese).
17. Phelps AS, Naeger DM, Courtier JL, et al. Pairwise comparison versus Likert scale for biomedical image assessment. *AJR Am J Roentgenol* 2015; 204:8–14.

18. Likert R. A technique for the measurement of attitudes. *Arch Psychol* 1932; 22:1–55.
19. Svanholm H, Starklint H, Gundersen HJ, Fabricius J, Barlebo H, Olsen S. Reproducibility of histomorphologic diagnoses with special reference to the kappa statistic. *APMIS* 1989; 97:689–698.
20. Eley KA, Watt-Smith SR, Sheerin F, Golding SJ. “Black Bone” MRI: a potential alternative to CT with three-dimensional reconstruction of the craniofacial skeleton in the diagnosis of craniosynostosis. *Eur Radiol* 2014; 24:2417–2426.
21. Robinson AJ, Blaser S, Vladimirov A, Drossman D, Chitayat D, Ryan G. Foetal “black bone” MRI: utility in assessment of the foetal spine. *Br J Radiol* 2015; 88:1046. doi:10.1259/bjr.20140496
22. Mastrogiacomo S, Dou W, Jansen JA, Walboomers XF. Magnetic resonance imaging of hard tissues and hard tissue engineered bio-substitutes. *Mol Imaging Biol* 2019. Apr 11. 2019. doi: 10.1007/s11307-019-01345-2. [Epub ahead of print]
23. Kadow T, Sowa G, Vo N, Kang JD. Molecular basis of intervertebral disc degeneration and herniations: what are the important translational questions? *Clin Orthop Relat Res* 2015; 473:1903–1912.
24. Widjaja E, Whitby EH, Paley MN, Griffiths PD. Normal fetal lumbar spine on postmortem MR imaging. *AJNR Am J Neuroradiol* 2006; 27:553–559.
25. Feng L, Benkert T, Block KT, Sodickson DK, Otazo R, Chandarana H. Compressed sensing for body MRI. *J Magn Reson Imaging* 2017; 45:966–987.
26. Lustig M, Donoho D, Pauly JM. Sparse MRI: the application of compressed sensing for rapid MR imaging. *Magn Reson Med* 2007; 58:1182–1195.
27. Zhang X, Xu Z, Jia N, et al. Denoising of 3D magnetic resonance images by using higher-order singular value decomposition. *Med Image Anal* 2015; 19:75–86.
28. Higaki T, Nakamura Y, Tatsugami F, Nakaura T, Awai K. Improvement of image quality at CT and MRI using deep learning. *Jpn J Radiol* 2019; 37:73–80.
29. Birkl C, Langkammer C, Golob-Schwarzl N, et al. Effects of formalin fixation and temperature on MR relaxation times in the human brain. *NMR Biomed* 2016; 29:458–465.
30. Buesa RJ, Peshkov MV. How much formalin is enough to fix tissues? *Ann Diagn Pathol* 2012; 16:202–209.
31. Haga Y, Hata J, Uematsu A, et al. MR imaging properties of ex vivo common marmoset brain after formaldehyde fixation. *Magn Reson Med Sci* 2019. Feb 7.2019. doi: 10.2463/mrms.mp.2018-0086. [Epub ahead of print]